Application of Transient IR Spectroscopy to Investigate the Role of Gold in Ethanol Gas Sensing over Au/SnO₂

Maximilian Pfeiffer, Christian Hess[*]

TU Darmstadt, Eduard Zintl Institute of Inorganic and Physical Chemistry, Alarich-Weiss-Str. 8, 64287 Darmstadt, Germany

*e-mail: christian.hess@tu-darmstadt.de

Abstract

Diffuse reflectance FTIR spectroscopy (DRIFTS) was used in combination with resistance measurements to study the mechanism of Au/SnO₂ during ethanol gas sensing and to elucidate the influence of gold on the sensor response. Time-resolved DRIFT spectra during ethanol gas sensing reveal significant differences between Au/SnO₂ and bare SnO₂ regarding the amount of C–H-containing adsorbates, which are less abundant on Au/SnO₂ due to their consumption by adsorbed oxygen species. Modulation excitation DRIFT spectroscopy (ME-DRIFTS) was applied to Au/SnO₂ in comparison to bare SnO₂, enabling a distinction of the temporal behavior of different C–H-containing surface adsorbates such as acetate and formate. ME-DRIFTS reveals the presence of a new surface species at 2030-2060 cm^{-1}, not detected for unloaded SnO₂ and associated with CO adsorbed on negatively charged gold particles. XP and UV/Vis spectra confirm the presence of metallic gold, which makes an influence on the electronic properties of the SnO₂ sensor material unlikely. Based on our spectroscopic findings, we postulate a detailed ethanol gas-sensing mechanism and attribute the increase in sensor response to an oxygen spillover from gold to the surface of tin oxide.

Keywords: Sensors, Tin oxide, Ethanol, Gold, IR Spectroscopy, Modulation Excitation Spectroscopy

TOC Graphic
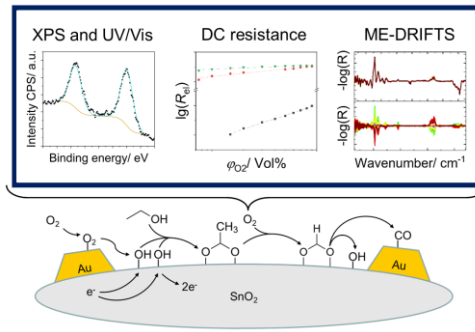
1. Introduction

Gas sensors are widely used in safety technology for the early detection of toxic and explosive gases in the ppm range. With the help of sensors, processes can be monitored, and thus limit values can be complied with.[1,2] In addition, the detection of gases such as CO and organic molecules plays an important role in the monitoring of exhaust gas emissions in the context of environmental protection. A widely used and well-studied sensing material with respect to ethanol gas sensing is tin oxide.[3-5] Its sensor properties can be significantly improved by adding noble metals such as platinum or gold.[6,7] Regarding the influence of noble metal loadings on the sensor response, chemical and electronic influences have been discussed in the literature. In particular two mechanisms, the spillover mechanism (chemical influence) and the Fermi-level control mechanism (electronic influence), have been used to explain the influence of noble metals on metal oxide gas sensors.[8,9] To a first approximation, one may assume either a dominant electronic or a dominant chemical influence of noble metals on the sensor response.[8,10]

The spillover-mechanism[8,10] describes a purely chemical influence of the noble metal, typically present as supported particles, leaving the support largely unchanged. Molecules adsorbed on the surface of the noble metal may be activated by electron transfer, followed by transport from the noble metal surface to the oxidic support across the metal/metal oxide interface.[11,12] For an exclusive spillover of the analyte, the latter is activated on the noble metal, leading to a change in reactivity. In the absence of the analyte, the surface of the metal oxide and the surface concentration of charged species remain unchanged, leaving the space charge region unchanged compared to the bare oxidic support. In the case of oxygen spillover, however, activation of the metal oxide surface occurs even in the absence of the analyte, as the concentration of charged oxygen species on the surface increases. Molecular oxygen ionosorbs on the noble metal, such as gold, before the spillover onto the metal oxide support occurs. This leads to an overall increase in surface reactivity and a more pronounced initial space charge zone due to band bending prior to exposure to the analyte.[11,13]

An electronic influence on the sensor response can be achieved by direct reaction of the noble metal with the metal oxide, either by forming a separate oxidic phase of the noble metal[14,15] or by being incorporated atomically as a dopant into the lattice of the metal oxide.[16] For an electronic effect, the reaction of the noble metal must change the electronic properties of the metal oxide by adjusting the space charge region. Since the original band bending of the metal oxide is changed by the electronic influence, independently of the gas atmosphere, prior to exposure to the analyte, the interaction with the noble metal leads to an improvement or deterioration of the response of the sensor material during exposure to the analyte.[8,9,17]

Previous studies have shown that *in situ* and *operando* Raman, UV-Vis and diffuse reflectance FTIR spectroscopy (DRIFTS) are powerful (non-invasive) methods for mechanistic studies on metal oxide gas sensors.[4,5,18] By combination of *operando* Raman/UV-Vis spectroscopy and gas-phase FTIR spectroscopy on tin oxide gas sensors, ELGER AND HESS were able to show that the sensing mechanism of tin dioxide during ethanol gas sensing is determined on the one hand by the formation and consumption of surface adsorbates and hydroxyl groups, and on the other hand by the formation of oxygen vacancies in the metal oxide.[5,18] In addition to ethoxy species, formate and acetate species were observed as surface adsorbates, and acetaldehyde, CO_2 and water as gas-phase products of the oxidation of ethanol.[5] These observations are in agreement with those obtained previously for indium oxide during ethanol gas sensing.[19] In addition to pure tin oxide, Au/SnO_2 has also been intensively investigated, especially for CO gas sensing, and the presence of a spillover mechanism was proposed.[11,13,20] The presence of electronic influences was excluded by work function and resistance measurements, as well as X-ray absorption near edge structure (XANES) spectroscopy.[6,13,21]

DRIFTS is particularly applicable to powdered samples and allows the *in situ* identification of adsorbates and other surface species by their vibrational bands. From the large number of different surface species, only a fraction is actively participating in the surface reaction. It is difficult to identify these active species as they are typically masked by spectator species. To isolate the active species from the spectator species, modulation excitation spectroscopy (MES) can be applied to DRIFT spectroscopy as a transient method by periodically varying a process variable, such as the analyte concentration.[22–26] During the modulation excitation, the investigated system is in a steady state when averaged over time, but is constantly disturbed by the modulation excitation and thereby brought out of the equilibrium state. The periodic excitation enables signals of observer and active species to be distinguished due to their response to the external modulation, because only active species react phase-shifted but with the same frequency as the external modulation.[23] By combining MES with the phase-sensitive detection (PSD) method, the masked active species can be identified and their dynamics can be studied.[22,24] Thus, applying this method provides detailed mechanistic insight, allowing us to establish new mechanisms or to extend existing ones, including reaction intermediates.

AGUIRRE AND COLLINS investigated the mechanism of the reverse water–gas shift reaction on Pd-doped γ-Ga_2O_3 catalysts by concentration modulation excitation DRIFT spectroscopy (ME-DRIFTS), including the influence of Pd-induced hydrogen spillover.[27] By applying ME-DRIFTS to γ-Al_2O_3 catalysts, SRINIVASAN *et al.* were able to elucidate differences in the reactivity of hydroxyl species towards ethanol.[24]

In the context of gas sensors, ME-DRIFTS has rarely been applied. The only study using ME spectroscopy on gas sensor materials known to us is by PAVELKO *et al.*, who investigated the influence of chloride traces on the CO-sensing mechanism of tin oxide by alternately pulsing CO-containing synthetic air streams, one of which was saturated with H_2O and the other with D_2O.[25] With this method, they constantly exchanged hydrogen isotopes on the sensor surface and so were able to determine the water adsorption kinetics on different synthesized tin oxides in a steady state. Although they used concentration modulation excitation by periodically switching between H_2O- and D_2O-containing atmospheres to reduce the signal-to-noise ratio of the DRIFT spectra, they did not apply PSD to the spectra obtained.[25]

For a detailed understanding of the influence of gold on the sensing properties of SnO_2, we have combined resistance measurements with structural characterization and transient IR spectroscopic methods. The data processing of the ME-DRIFT spectra was improved by performing a background subtraction for all acquired spectra to minimize broad background features, which interfere with the PSD. This allows the applicability of the ME-DRIFTS method to be extended to sensor and catalyst materials. We highlight the potential of ME-DRIFTS for detailed mechanistic studies on gas sensors.

2. Experimental

2.1 Material Preparation. In this work, we used commercial tin(IV) oxide SnO_2 (Sigma Aldrich) with a purity of 99.9% and ~325 mesh. To remove impurities from long-term storage, the tin oxide was calcined at 600°C with a heating rate of 2°C/min for 12 h in a chamber furnace, crushed in a mortar and sieved (mesh size: 56 μm).

As a precursor for the gold loading of tin oxide, we employed tetrachlorogold(III) acid, $HAuCl_4 \cdot 3H_2O$ (Carl Roth, 99.9% purity metal basis). For a 0.5 wt% gold loading, 1.00 g SnO_2 was dispersed in 254 mL of 1 mM aqueous $HAuCl_4$ solution by stirring and ultrasonication for 15 min. Afterwards, 55 mL of 30 mM aqueous ammonia solution was added at room temperature for 1 h until a pH value of 9.25 was reached. The pH value was monitored with a pH electrode.

After addition of the ammonia solution, stirring was continued for 2 h at room temperature. Then the obtained purple suspension was dispersed again for 30 min in an ultrasonic bath. The resulting solid was centrifuged at 8000 rpm for 5 min, the supernatant was discarded, and the residue was washed four times with distilled water. The remaining residue was dried for 16 h at 85°C in a drying chamber, followed by calcination for 3 h at 300°C in a chamber oven (heating rate: $2°C \cdot min^{-1}$). The resulting solid was crushed in a mortar and sieved (mesh size: 56 μm).

2.2 Structural Characterization and *in situ* Spectroscopy. Diffuse reflectance UV-Vis spectra were recorded on a Jasco V-770 UV-Vis/NIR spectrophotometer, equipped with a heatable Praying Mantis gas cell (Praying Mantis High Temperature, Harrick Scientific Products) and a Peltier-cooled PbS detector. A halogen lamp and a deuterium lamp served as radiation sources for excitation. Spectra were recorded within the range 200-1000 nm with a resolution of 1 nm, averaged over three individual measurements per spectrum. MgO was used as a white standard.

X-ray photoelectron (XP) spectra were recorded on an SSX 100 ESCA spectrometer (Surface Science Laboratories Inc.) under high vacuum conditions, using monochromatic Al K_α radiation. The spot size was 0.25×1.00 mm^2. To minimize charging effects, an electron flood gun with an energy of 0.5 eV was employed. XP spectra were recorded at room temperature with a step size of 0.05 eV and analyzed using Casa XPS software. Binding energies were calibrated based on the 4f signal of gold foil at 84.0 eV and the Cu 2p signal of a copper plate at 932.7 eV.

For X-ray diffraction measurements we employed an X-ray powder diffractometer (StadiP, Stoe & Cie GmbH) in transmission geometry, using Cu $K_{\alpha1}$ ($\lambda = 1.5406$ Å; Ge[111]-monochromator) radiation, and a Mythen 1K (Dectris) detector.

A Vertex 70 IR spectrometer (Bruker) with a liquid nitrogen cooled MCT detector was used to record the time-resolved DRIFTS spectra and perform the modulation excitation measurements.

The spectrometer was equipped with a heatable Praying Mantis gas cell (Praying Mantis High Temperature, Harrick Scientific Products). The sample was placed on flat stainless-steel sample plates with a diameter of 8 mm and a depth of 0.5 mm; the sample mass was about 25 mg. The sample temperature was calibrated by inserting a thermocouple inside a ceria sample bed placed on an equal sample plate as described above. During the calibration procedure, it was ensured, that the thermocouple did not touch the sample plate. From this data, a calibration curve was determined, which was used for all measurements. The measurement cell was closed by a dome which, in addition to a quartz glass window, included two ZnSe windows (time-resolved measurements) or, alternatively, two KBr windows (modulation excitation measurements). The total gas flow was set to 80 mL·min^{-1}. As a reference for the calculation of -log(R), we recorded spectra of the respective samples at room temperature using synthetic air as a carrier gas. For quantitative analysis of the exhaust gas from the *in situ* DRIFTS measurements, a Tensor27 FTIR spectrometer (Bruker) was used, which was equipped with a silicon carbide pin as the MIR source, a DLaTGS pyroelectric detector and an LFT 205-20 gas cell (Axiom Analytical Incorporated).

For the time-resolved DRIFTS measurements, a fixed sequence of different conditions was applied at each operating temperature, which was increased stepwise from 100°C to 325°C. The sequence was started with a pretreatment at 400°C in synthetic air for 20 min at a flow rate of 80 mL·min^{-1}. The material was then cooled to the respective operating temperature in synthetic air or nitrogen (carrier gas) and treated for 10 min. Afterwards, 500 ppm ethanol was added to the corresponding carrier gas for 20 min. Finally, the addition of ethanol was stopped but the flow of the corresponding carrier gas was maintained for another 10 min before the sample was heated again to 400°C for 20 min in synthetic air to start the next sequence at the next temperature.

2.3 Resistance measurements. For sensor preparation, the tin oxide-based samples (30 mg) were ultrasonically dispersed in deionized water and then applied in drops to the surface of an Al_2O_3-transducer substrate with interdigitated Pt electrodes (electrode separation ~150 μm) to measure the sensor resistance R_{el}. On the other side of the substrate, a meander Pt heater was printed to heat the sensing material. The sensor resistance R_{el} was measured using a Keithley 2000 Multimeter. The temperature of the Pt heater was calibrated prior to experiments. For resistance measurements, the following gases (Westfalen AG) were used: oxygen 5.0 ($\leq$0.2 ppm CO_2, $\leq$ 0.2 ppm C_nH_m, $\leq$3 ppm H_2O, $\leq$10 ppm N_2+Ar), nitrogen 5.0 ($\leq$ 3 ppm O_2, $\leq$ 1 ppm C_nH_m, $\leq$ 5 ppm H_2O), and 1000 ppm ethanol in nitrogen 5.0. To measure the sensor response S (see equation 1), the carrier gas used was synthetic air or nitrogen cycled with 500 ppm ethanol in synthetic air or nitrogen fed at 80 mL·min^{-1}. Here, $R_{SA/N2}$ is the sensor resistance before the ethanol addition in the carrier gas synthetic air (SA) or nitrogen (N2) and R_{EtOH} the sensor resistance during ethanol addition.

$$S = \frac{R_{\text{SA/N2}}}{R_{\text{EtOH}}} \qquad (1)$$

To measure the resistance as a function of the oxygen fraction, a total flow rate of 100 mL·min⁻¹ with nitrogen as a carrier gas was used and the volume fraction of oxygen was increased stepwise from 7.5 Vol% to 90 Vol%.

2.4 Modulation Excitation Spectroscopy and Data Acquisition. The sensor was modulated by periodically adding 500 ppm ethanol to synthetic air, using a four-way valve. Figure 1 depicts the experimental setup of ME-DRIFTS used for measurements on gas sensors, including the gas-supply system and the four-way valve.
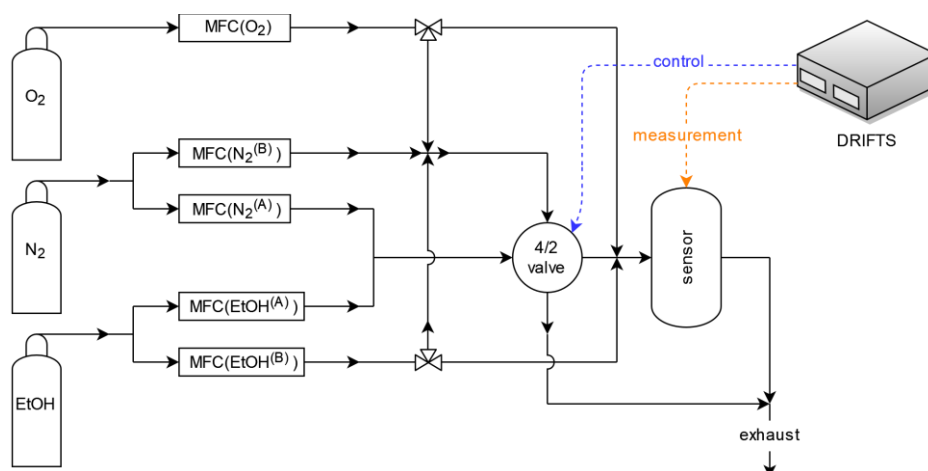
Figure 1. Schematic setup of ME-DRIFTS applied to gas sensors, including the gas-supply system, four-way valve and sensor; A and B correspond to alternating gas mixtures passing the 4/2-valve.

Before each modulation excitation experiment, the sensor material was pretreated for 20 min in synthetic air at the same temperature as used for the experiment (total flow rate: 80 mL·min⁻¹). During one modulation cycle (exposure to 500 ppm ethanol in synthetic air followed by an equally long exposure to synthetic air), 60 infrared spectra were recorded at 40 kHz sampling rate using the rapid scan acquisition mode of the FTIR spectrometer. For each spectrum, 5-10 scans were averaged and so a new spectrum was recorded every 2.2 s.). One modulation cycle can be divided into two half-periods of equal length (66.66 s). During the first half-period, ethanol in synthetic air flows and during the second half-period, just synthetic air. The first ten modulation period cycles of each modulation excitation experiment were excluded from further data processing. The

IR spectra of the remaining modulation periods were averaged over 15-20 periods. The resulting time-resolved IR spectra were demodulated with PSD according to equation 2:

$$I\left(\tilde{v}, \Phi^{\mathrm{PSD}}\right) = \frac{2}{T_{\mathrm{t}}} \cdot \int_{t_{\mathrm{cutoff}}}^{t_{\mathrm{end}}} I(\tilde{v}, t) \cdot \sin\left(\omega \cdot t + \Phi^{\mathrm{PSD}}\right) dt \qquad (2)$$

Here $\tilde{v}$ is the wavenumber, ω the stimulation frequency, T_{t} the duration of one modulation period, and Φ^{PSD} the demodulation phase angle. With one set of time-resolved spectra, equation 2 can be evaluated for different phase angles Φ^{PSD}, resulting in a series of phase-resolved absorbance spectra. The obtained phase angles Φ^{PSD} can also be converted back into a time value Δt within a period using the duration of one modulation period T_{t} via equation 3.

$$\Delta t = T_{\mathrm{t}} \cdot \left(1 - \frac{\varphi_{\mathrm{max}}}{360°}\right) \qquad (3)$$

For the calculation of the time values Δt, 360 PSD spectra were calculated, corresponding to a phase angle spacing of the PSD spectra of 1°. Hence, one PSD spectrum was calculated for each time span of 0.37 s ($T_{\mathrm{t}} = 133.33$ s). A more detailed description of the modulation excitation technique and PSD can be found elsewhere.[23,28]

3. Results and General Discussion

The sensor materials used were characterized by inductively coupled plasma optical emission spectrometry (ICP-OES) to determine their composition, by X-ray diffraction (XRD) to identify changes in the material phases, and by BET (Brunauer–Emmett–Teller) measurements to determine their specific surface area. The results of the ICP-OES and BET measurements are listed in Tables S1 and S2, and the diffractograms obtained by XRD are shown in Figure S1. All materials show reflex positions resembling those of a SnO_2 reference. The mean crystallite size d of the tin oxide samples was determined from the full width at half maximum (FWHM) by applying the Scherrer equation,[29] yielding a value of 58 nm. Reflexes for metallic gold were not observed due to the low mass fraction of gold in the materials. The mass fraction of gold, determined by ICP-OES, ranges from 0.04 wt% to 0.56 wt% Au.

To further characterize the gold-loaded materials, XP and diffuse reflectance UV-Vis spectroscopy were used. Figure 2a) shows the Au 4f photoemission of 0.56 wt% Au/SnO_2. Peak fitting of the Au 4f signals reveals the exclusive presence of metallic gold, without an indication of cationic gold, which would show bands shifted to higher binding energies.[30] UV-Vis spectra of bare tin oxide and tin oxides loaded with different amounts of gold were acquired to further investigate the influence of gold on the electronic properties of the sensor material. As depicted in Figure 2b), compared to the UV-Vis spectrum of bare SnO_2 discussed previously,[5] the gold-loaded samples are characterized by a new broad band at about 550 nm, which shows an intensity increase and a red shift with increasing gold loading. Based on the observed behavior, we attribute the 550 nm band to the surface plasmon resonance of metallic gold,[31] while the red shift is consistent with the reported shift of the plasmon resonance with increasing particle size.[32]

Apart from the surface plasmon resonance, no significant changes in the absorption maximum and absorption edge were observed in the UV-Vis spectra of the Au/SnO_2 samples compared to bare SnO_2.
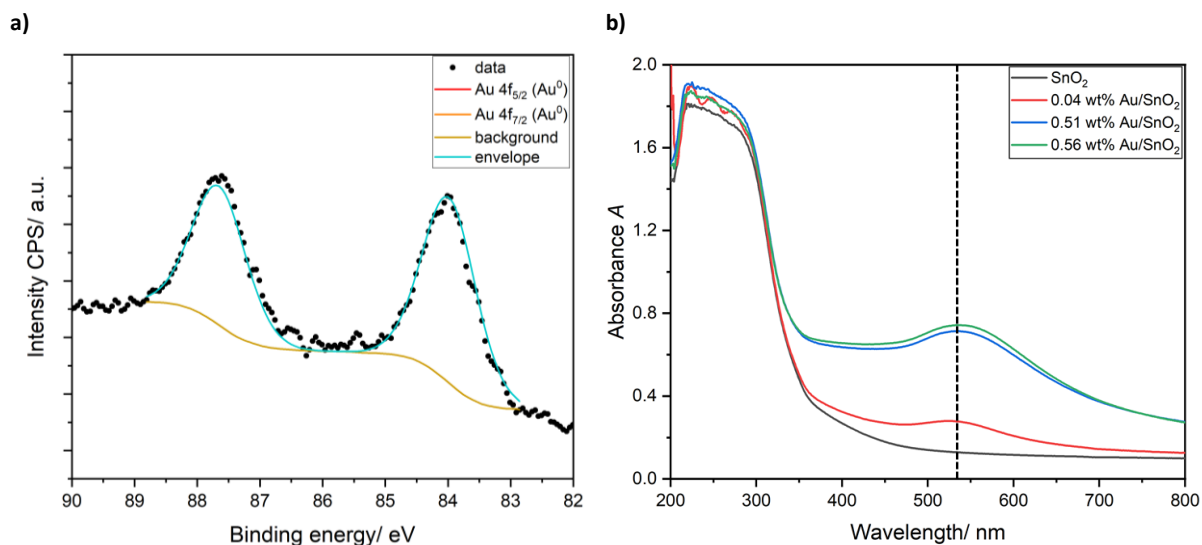
Figure 2. a) Au 4f photoemission of 0.56 wt% Au/SnO$_2$ together with the results from a fit analysis. b) Diffuse reflectance UV-Vis spectra of bare and gold-loaded SnO$_2$. The vertical line at 530 nm illustrates the red shift of the surface plasmon resonance with increasing gold loading.

Figure 3a) presents the sensor responses *S* for bare tin oxide and two gold-loaded tin oxides when exposed to 500 ppm ethanol in synthetic air for temperatures between 100°C and 325°C. Bare tin oxide shows a decrease in the sensor response *S* with increasing operating temperature. In contrast, the sensor response *S* of the gold-loaded tin oxides first declines, then passes through a maximum, and finally decreases. With increasing gold loading, the maximum sensor response shifts to lower operating temperature. Furthermore, the sensor response *S* increased with increasing gold loading, especially within the range 150-300°C for 0.56 wt% Au/SnO$_2$. Figure 3b) depicts the corresponding resistance values R_{el} after 18 min exposure to 500 ppm ethanol in synthetic air. Both gold-loaded samples showed a noticeably higher resistance during ethanol exposure than bare SnO$_2$. However, the basic course of resistance with increasing temperature was quite similar. A minimum of resistance was reached at about 230-300°C, while the resistance increased again at higher temperatures.
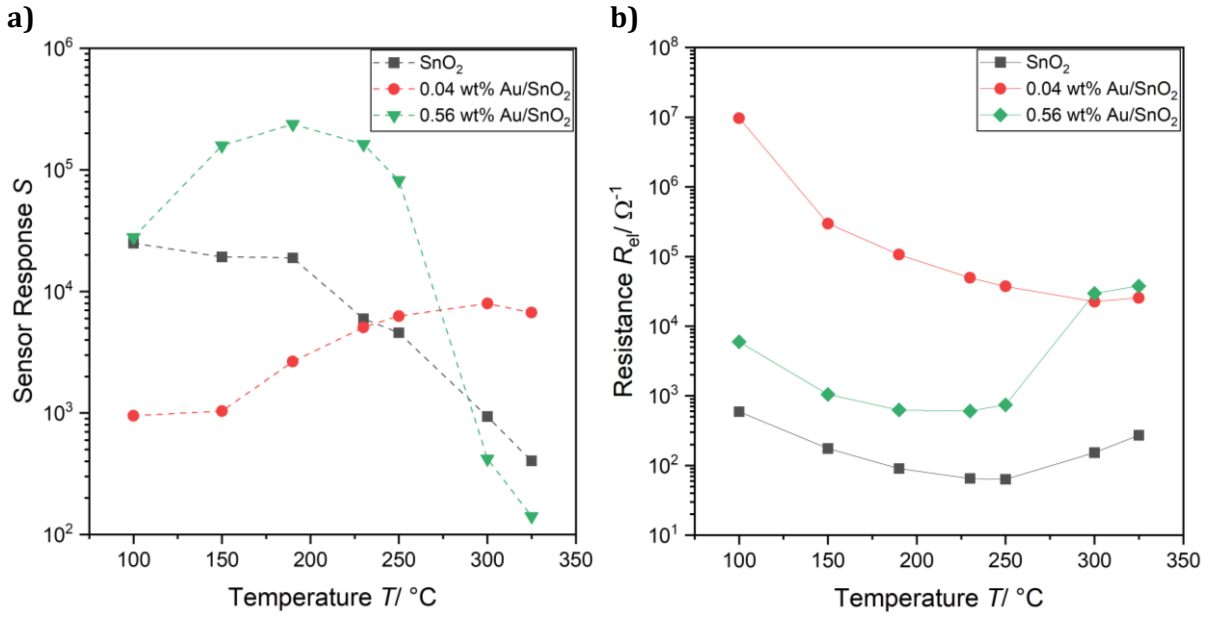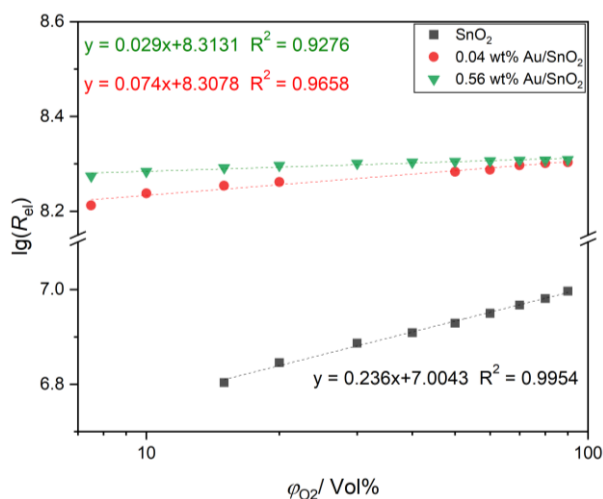
Figure 3. a) Sensor response S for SnO_2 and gold-loaded SnO_2, exposed to 500 ppm ethanol in synthetic air, as a function of temperature. b) Corresponding resistance R_{el} after 18 min of exposure to 500 ppm ethanol in synthetic air.

To investigate the influence of oxygen on the sensor response S as a function of the gold loading in more detail, the volume fraction of oxygen in the gas phase was successively increased from 7.5 Vol% to 90 Vol% O_2 with nitrogen as the carrier gas at an operating temperature of 150°C. Considering the equilibrium reaction shown in equation 4, a linear relationship between the logarithm of the resistance R_{el} and the logarithm of the volume fraction of oxygen φ_{O2} (equation 6) can be established by using equation 5, assuming the volume fraction φ_{O2} to be approximately proportional to the oxygen partial pressure p_{O2} using the ideal gas law. The derivation of equations 4 to 6 can be found elsewhere.[33,34]

$$V_O^{\cdot\cdot} + \frac{1}{2}O_{2,\text{gas}} + 2e'(\text{CB}) \rightleftharpoons O_{O,\text{surf}}^{x} \tag{4}$$
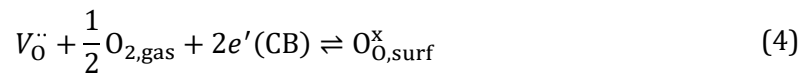
$$\frac{1}{R_{el}} \sim p_{O2}^{-n} \tag{5}$$

$$\ln R_{el} = n \cdot \ln p_{O2} + b \tag{6}$$

Figure 4. Double logarithmic plot of the sensor resistance R_{el} against the volume fraction of oxygen in the gas-phase φ_{O2} for SnO_2 and gold-loaded SnO_2 at a temperature of 150°C. Oxygen mixed with nitrogen, total flow rate: 80 mL·min⁻¹.

As shown in Figure 4, the sensor resistance of unloaded and loaded SnO_2 follows the linear behavior predicted by equation 6. With increasing gold loading, a decrease in the slope *n* of the regression line and an increase in the measured resistances was observed. The resistance of the gold-loaded samples was an order of magnitude higher than that of bare SnO_2. Summarizing the results of the resistance measurements in Figs. 3 and 4, a distinct effect of gold on the sensing properties of SnO_2 is observed, which will be further discussed in Section 4.

In the following, the results of the time-resolved DRIFTS measurements will be presented. For the DRIFTS measurements, the sensor material was treated with a sequence of different gas compositions (see Experimental) at the same operating temperatures as used to determine the sensor response *S*. An example overview DRIFT spectrum of sample 0.56 wt% Au/SnO_2 during exposure to 500 ppm ethanol in synthetic air at an operating temperature of 150°C is shown in Figure S2. The most important band assignments for the DRIFT spectra obtained by time-resolved DRIFT spectroscopy and ME-DRIFTS are summarized in Table S3.

The time-resolved DRIFTS measurements of the sensor samples were coupled with simultaneous gas phase FTIR spectroscopy to monitor the gas-phase composition. During exposure to ethanol, CO_2, ethanol, acetaldehyde and water were observed as gas-phase products, whereas upon heating to 400°C after ethanol exposure only CO_2 and water were detected. There was no indication of other possible gas-phase products such as CO, methane and ethylene.

To investigate the dynamics of selected bands of the sensor material in response to the applied sequences, first a background subtraction and then an integration were performed. Figures 5–7 show the time-dependent evolution of the resulting band intensities.

13

Figure 5 depicts the accumulated intensity of the OH bands within the range 3450 cm^{-1}-3800 cm^{-1} for bare SnO_2 and 0.56 wt% Au/SnO_2 when using synthetic air (see Figure 5a) and nitrogen (see Figure 5b) as the carrier gas.
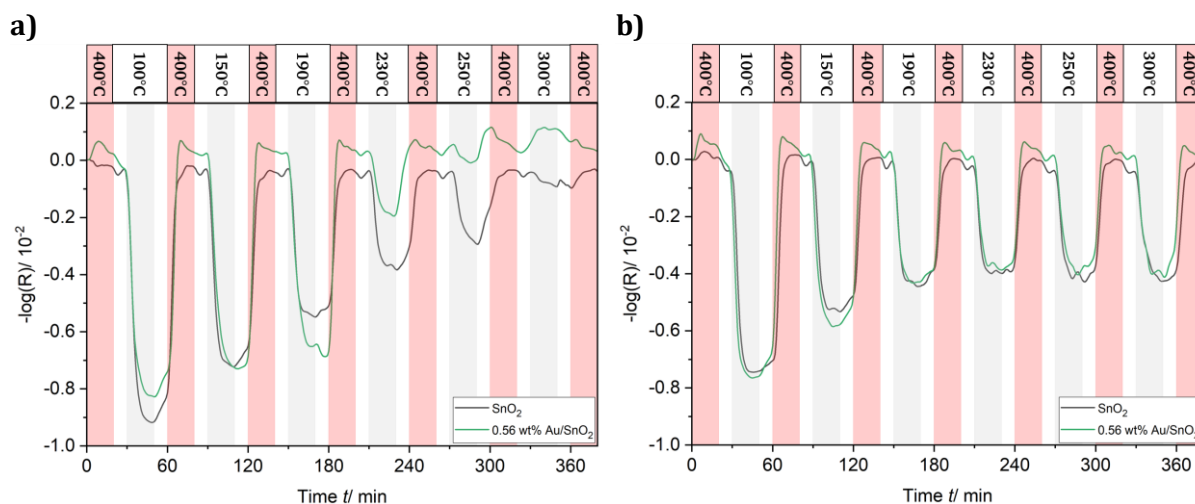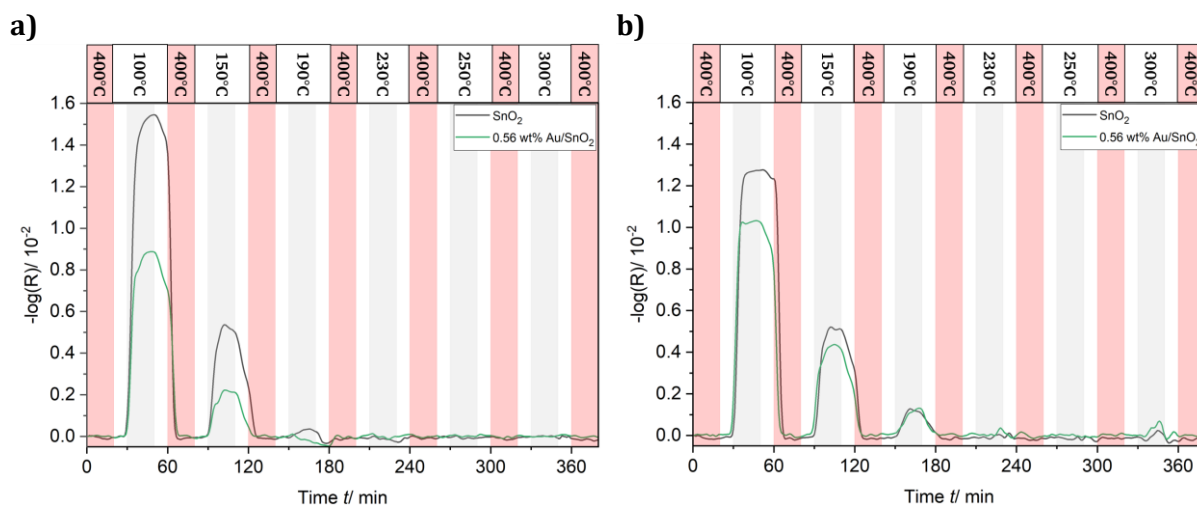

Figure 5. Accumulated DRIFTS-intensity of the OH bands in (a) synthetic air and (b) nitrogen as a carrier gas for bare SnO_2 and 0.56 wt% Au/SnO_2; red areas: heating at 400°C in synthetic air; white areas: sensor at operating temperature in the respective carrier gas; grey areas: exposure to 500 ppm ethanol in the respective carrier gas; total flow rate: 80 mL·min^{-1}.

During the exposure to synthetic air (see Figure 5a), the gold-loaded sample shows a weaker decrease in intensity than the unloaded sample at all temperatures. It is also noticeable that the intensity for the gold-loaded sample became even positive in the presence of ethanol at higher temperatures. Such a behavior was not observed outside the heating phases when using nitrogen as the carrier gas (see Figure 5b). The gold-loaded sample showed a similar band intensity curve to the unloaded sample. Hereby, the band curve is only slightly shifted compared to the band curve of bare tin oxide.

Differences in the spectral behavior during ethanol exposure can also be observed for the integrated intensity of the 2969 cm^{-1} band, shown here as a representative for all C–H-containing adsorbates (see Table S3), both in synthetic air (see Figure 6a) and in nitrogen (see Figure 6b). In both carrier gases, the intensity follows a very similar course, showing an increase during ethanol exposure up to a maximum at the beginning of the regeneration phase, where ethanol is switched off, followed by a slight intensity decrease (see white areas), which is greater in synthetic air than in nitrogen because of partial adsorbate oxidation and the complete disappearance of intensity with the onset of heating to 400°C. For the loaded and unloaded samples similar behavior is observed, except for the maximum intensity, which decreased upon gold loading, both in synthetic air and in nitrogen. This decrease is smaller in nitrogen than in synthetic air, providing a first

indication that the influence of gold on the sensing mechanism and the corresponding spectral bands may be more pronounced in the presence of oxygen.


Figure 6. DRIFTS intensity of the 2969 cm^{-1} band ($\nu(CH_3)$) in (a) synthetic air and (b) nitrogen as a carrier gas for bare SnO_2 and 0.56 wt% Au/SnO_2; red areas: heating at 400°C in synthetic air; white areas: sensor at operating temperature in the respective carrier gas; grey areas: exposure to 500 ppm ethanol in the respective carrier gas; total flow rate: 80 mL·min^{-1}.

Besides the accumulated OH and adsorbate-related bands, also the band at 934 cm^{-1}, which can be assigned to a deformation vibration of a terminal surface hydroxy group $\delta(Sn-OH)$,[4,35,36] shows differences for unloaded and gold-loaded samples. A comparison of Figure 7a and b shows that the integrated intensity was lower for the gold-loaded sample than for the unloaded sample during 400°C treatment and ethanol exposure. On the other hand, the gold-loaded samples showed a stronger intensity increase during the regeneration phases, which was more pronounced in the presence of oxygen. Based on the results of Figure 7a, we can conclude that the presence of gold in combination with oxygen in the gas phase facilitates consumption of specific terminal hydroxy groups during ethanol exposure as well as their regeneration.
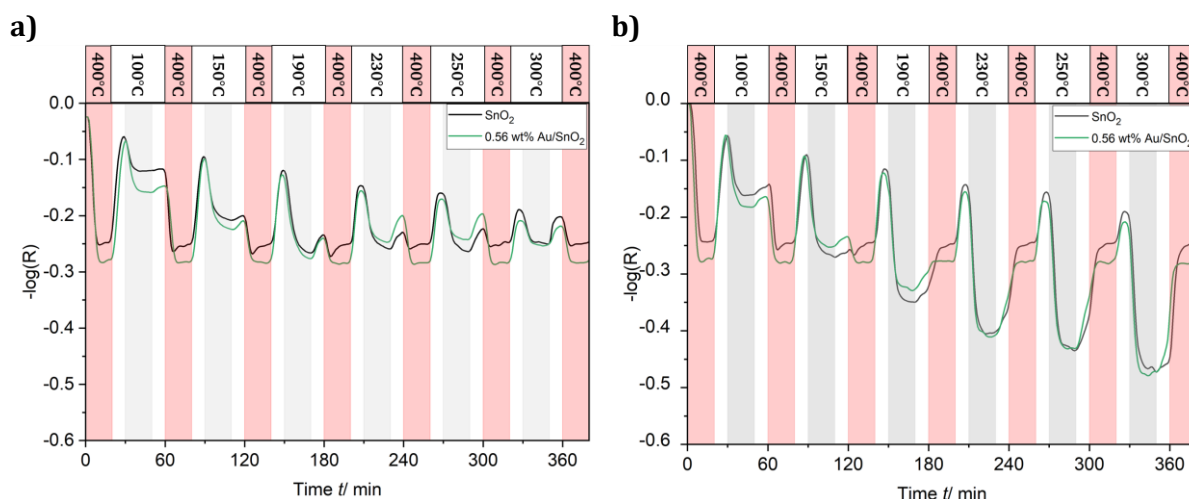
Figure 7. DRIFTS-intensity of the 934 cm^{-1} band (δ(Sn-OH)) in (a) synthetic air and (b) nitrogen as a carrier gas for bare SnO$_2$ and 0.56 wt% Au/SnO$_2$; red areas: heating at 400°C in synthetic air; white areas: sensor at operating temperature in the respective carrier gas; grey areas: exposure to 500 ppm ethanol in the respective carrier gas; total flow rate: 80 mL·min^{-1}.

Next, we employed ME-DRIFTS in combination with PSD to identify active species during ethanol gas sensing and to gain more detailed insight into the role of gold. Figure 8 illustrates the data processing steps including PSD and background subtraction. Based on the time-resolved spectra in Figure 8a, which were averaged over 15 periods, only minor differences can be identified. The spectra are rather dominated by a broad mid-IR absorption, which hampers a more detailed analysis of individual band changes.
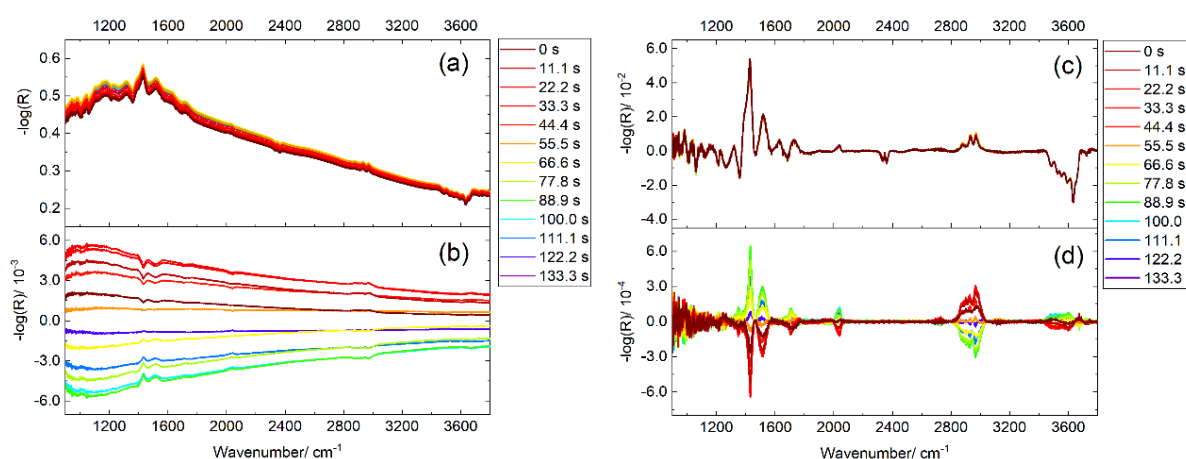
Figure 8. ME-DRIFTS data for pulsing 500 ppm ethanol in synthetic air over 0.56 wt% Au/SnO$_2$ at 150°C. (a) Time-resolved spectra averaged over all periods, (b) PSD spectra without background subtraction, (c) Time-resolved spectra with background subtraction averaged over all periods, (d) PSD spectra with background subtraction. Total flow rate: 80 mL·min^{-1}.

Figure 8b) presents the PSD spectra obtained from the time-resolved spectra in Figure 8a). Again, the spectra are dominated by the broad mid-IR absorption and its changes during the modulation excitation. Despite the use of the MES-PSD approach, the active species were masked. We

16

therefore performed a background subtraction for each of the time-resolved spectra to allow the observation of the active species despite the broad mid-IR absorption. The corrected spectra after background subtraction are shown in Figure 8c) and those after application of PSD in Figure 8d). As intended, the new PSD spectra show a horizontal baseline from which the bands of active species emerge.

To elucidate the influence of gold on the mechanism of ethanol gas sensing over tin oxide, we performed MES measurements for bare and gold-loaded SnO_2 under otherwise identical conditions. Sections of the corresponding PSD spectra, recorded during pulsing of 500ppm ethanol at 150°C, are presented in the top (SnO_2) and middle (0.56 wt% Au/SnO_2) panel of Figure 9. These were used to calculate PSD difference spectra (bottom panel), by subtracting the PSD spectrum of bare SnO_2 from that of Au/SnO_2 at each time point during a period. It should be mentioned that this procedure led to the same results as forming difference spectra of the time-resolved spectra and then performing the PSD. Please note, that this type of difference spectra should be interpreted with caution and only in connection with the spectra, from which they are calculated. Only bands, which appear exclusively in one of the spectra, or differences between bands with the same band maximum, which appear in both spectra, should be interpreted. New bands, which appear only in the difference spectra, but not in the original spectra, should not be considered for interpretation. Difference bands of bands, which result from very weak features, should also be discarded, as well as differences of bands from very noisy regions of the spectra. If these guidelines are considered, difference PSD spectra may provide additional information on the influence of surface loading on the surface reactions. It is expected that especially at low surface loadings the use of substrate PSD spectra as background spectra is a suitable approximation allowing the influence of the surface loading to be isolated.

The band assignments of the most important vibration bands are summarized in Table S3.
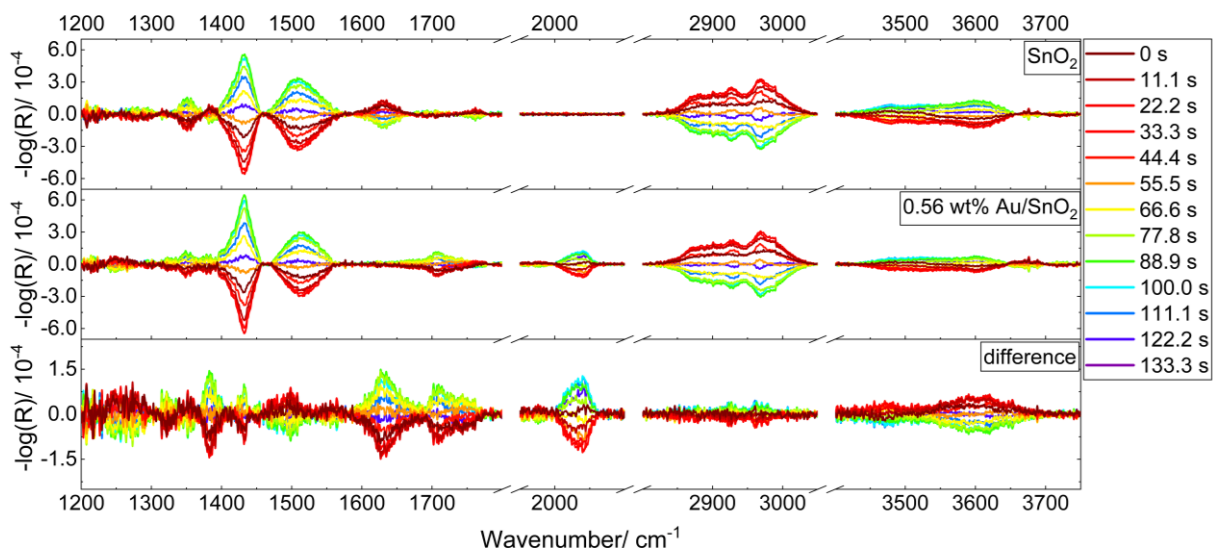
Figure 9. PSD spectra with background subtraction for bare SnO$_2$ (top) and 0.56 wt% Au/SnO$_2$ (middle) during pulsing 500 ppm ethanol in synthetic air at 150°C. At the bottom the corresponding PSD difference spectrum (Au/SnO$_2$ – SnO$_2$) is shown. Total flow rate: 80 mL·min^{-1}.

Inspection of the PSD spectra of the two materials and the difference PSD spectra reveals significant differences regarding the intensity and dynamics of individual bands. For gold-loaded tin oxide, a new band is observed at 1705 cm^{-1}, which has been assigned to the ν(C=O) stretching vibration of acetaldehyde.[37] The δ(HOH) deformation vibration of water[4] observed at 1626 cm^{-1} can be detected for bare tin oxide, but not for gold-loaded tin oxide. The bands at 1379 cm^{-1} and 1432 cm^{-1} were slightly more pronounced for the gold-loaded sample than for the unloaded sample, whereas the bands at 1349 cm^{-1} and 1515 cm^{-1} were slightly weaker. The bands at 1379 cm^{-1} and 1432 cm^{-1} can be assigned to surface carbonates,[3,36,38,39] and the bands at 1349 cm^{-1} and 1515 cm^{-1} to surface carboxylates.[3,38,39] Principally, the bands at 1349, 1432 and 1515 cm^{-1} could alternatively be assigned to acetate species. The band at 1349 cm^{-1} would be related to the δ(CH$_3$) vibration, the band at 1432 cm^{-1} to the ν$_s$(OCO) vibration, and the band at 1515 cm^{-1} to the ν$_{as}$(OCO) vibration[40]. These bands have previously been observed for the adsorption of acetic acid on tin oxide[41]. However, in the context of this work, the assignment of acetate to this synchronic appearing bands can be safely excluded based on a comparison to the behavior of the bands between 2850 cm^{-1} and 3000 cm^{-1}, which can be clearly assigned to the ν(C-H) vibrations of ethanol, acetate and formate. These bands show there maxima in the PSD spectra during the first half period, where ethanol is exposed to tin oxide. In contrast, the bands at 1349, 1432 and 1515 cm^{-1} do not show their maxima until the second half-period. Thus, they cannot be assigned to the same species and the assignment to carbonates and carboxylates is more likely. A contribution of Sn-O-Sn overtones to the bands at 1349, 1379, 1432 and 1515 cm^{-1} cannot be excluded based on the results presented here.[35,42]

At about 2040 cm^{-1}, gold-loaded tin oxide shows a new band, which is not detected for bare tin oxide and which shows its maximum intensity after about 100 s in the second half-period following the end of ethanol exposure. We attribute this band to CO adsorbed on negatively charged gold particles (CO-Au$^{\delta-}$),[43–45] based on a comparison of the band position with those reported for conceivable surface species on gold such as CO, oxygen,[46] ethanol,[47] acetaldehyde,[48] ethylene,[49] water,[50] hydrogen,[51] carboxylates or carbonates.[48,52] The new band at 2040 cm^{-1} exhibits an asymmetric profile that can be decomposed into two contributions at 2030 cm^{-1} and 2040 cm^{-1}. The time-shifted appearance of the two sub-bands may indicate a transition from a kinetically preferred (2030 cm^{-1}) to a thermodynamically more stable surface species (2040 cm^{-1}), as discussed below.

The ethanol, acetate and formate bands[5] present in the ν(C-H) range from 2850 cm^{-1} to 3000 cm^{-1} (see table S3) show a slightly smaller intensity change for the gold-loaded sample compared to bare tin oxide. A band at around 1100 cm^{-1} should be expected for the ν(C-O) vibration of ethoxy[53,54] but was not observed in the PSD spectra, neither for both bare nor gold-loaded tin oxide. However, such a feature was observed in the DRIFT spectra recorded during ethanol exposure with concentration modulation at 100 to 190 °C, besides the δ(CH$_3$) vibration of ethanol and ethoxy[37,43] at around 1390 cm^{-1} (see Figure S2). This band could not be clearly observed in the PSD spectra. The band expected at 1100 cm^{-1} occurs in a region of the PSD spectra, where the signal-to noise ratio is too low for a reliable differentiation between bands. The expected band at 1390 cm^{-1} for the δ(CH$_3$) vibration seems to overlap with the band of carbonate and carboxylates as well as the suggested contributions of Sn-O-Sn overtones. Thus, it cannot be differentiated from the bands of carboxylates and carbonates in the PSD spectra.

Within 3450 cm^{-1} to 3800 cm^{-1} differences in the magnitude of the intensity changes were observed, resulting mainly from ν(OH) stretching vibrations. While differences were small for wavenumbers >3650 cm^{-1} and hardly present for >3700 cm^{-1}, significant differences were detected between 3450 cm^{-1} and 3650 cm^{-1}, which were smaller for the gold-loaded tin oxide than for bare tin oxide.

In order to investigate the dynamics of selected bands and identify overlapping sub-bands of slightly different time values within broader band groups, we determined for selected wavenumbers the time values Δt within a period at which their maximum intensity was observed (see equation 3). As shown in Figure 10, besides the 2040 cm^{-1} band, the two ranges 2850-3050 cm^{-1} and 3450-3650 cm^{-1} were considered for analysis. The upper panel of Figure 10 depicts the sections of the PSD spectrum examined for the 0.56 wt% Au/SnO$_2$ sample, recorded during pulsing of 500 ppm ethanol in synthetic air at 150°C, while the lower panel presents the corresponding time values for the maximum band intensity as described above.

The maximum of the new band at about 2040 cm^{-1} appears after about 100 s and shifts with increasing time from about 2030 cm^{-1} (100.0 s) to 2040 cm^{-1} (102.5 s), indicating that the species corresponding to the lower wavenumber position transforms into a species characterized by a higher wavenumber.
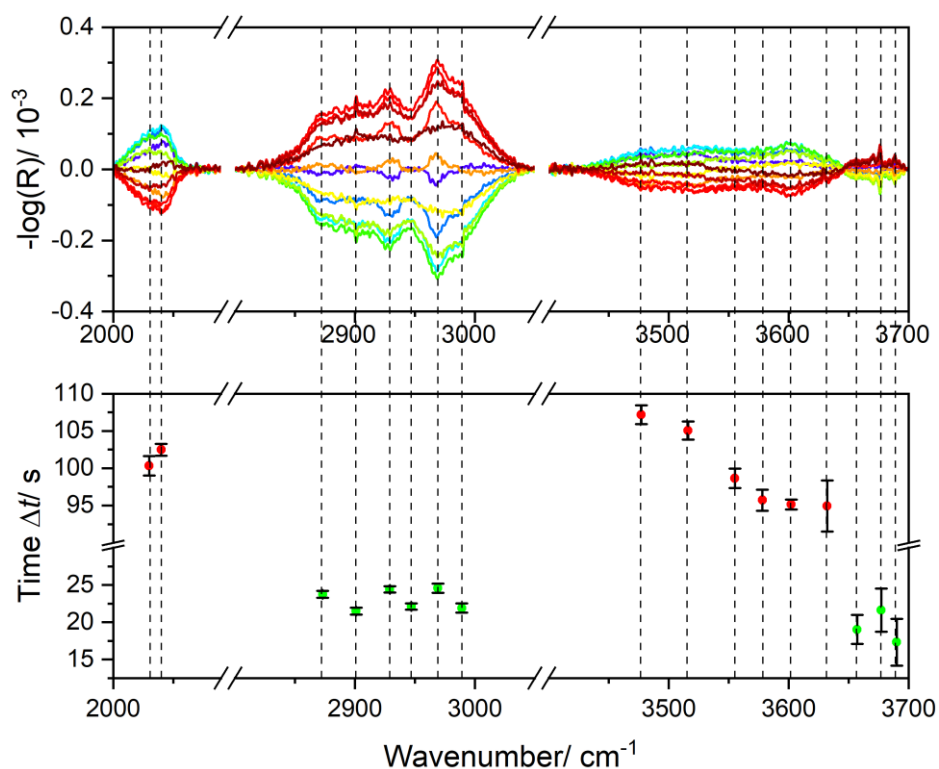
Figure 10. Temporal analysis of selected wavenumber ranges in the PSD spectra for 0.56 wt% Au/SnO$_2$ during pulsing of 500 ppm ethanol in synthetic air at 150°C. Time values Δt (bottom panel) were calculated from the phase angles at maximum band intensity. Dashed lines indicate the maxima of observed features and their corresponding time values. Time values in the first half-period are colored green, while those in the second half-period are colored red. The error bars show the standard deviation of the time values Δt within a range of ±5 cm^{-1} with respect to the position of the maximum.

For the ν(C-H) stretching vibrations within the range from 2850 cm^{-1} to 3050 cm^{-1} (see Table S3), different time values Δt were determined. In fact, the features at 2873 cm^{-1}, 2929 cm^{-1}, and 2969 cm^{-1} (see Figure 10) reached their maxima after about 24.2±0.9 s, i.e., about 2.4 s after the band fractions at 2901 cm^{-1}, 2947 cm^{-1}, and 2989 cm^{-1}. This difference in time values Δt is significant because the difference in time values is greater than both the step size of the PSD with respect to time values (0.37 s) and the time interval between two recorded DRIFT spectra (2.2 s). Also, there is no overlap of the error bars, which correspond to the standard deviation of the time values within a range of ±5cm^{-1} with respect to the position of the maximum.

The bands at 2901 cm^{-1}, 2947 cm^{-1}, and 2989 cm^{-1} have been assigned to stretching vibrations of adsorbed ethanol,[5,37,43,55] whereas the bands at 2873 cm^{-1}, 2929 cm^{-1}, and 2969 cm^{-1} can be

attributed to stretching vibrations of ethoxy and the products of the partial oxidation of ethanol and ethoxy such as acetate or formate.[5,37,43,55] Thus, the appearance of IR features of adsorbed ethanol precedes those of ethoxy, acetate and formate species, which are formed by consumption of ethanol. Furthermore, CO is formed delayed with respect to acetate, formate and other possible reaction products such as carboxylates and carbonates.

In the hydroxyl region (3400-3800 cm^{-1}, see table S3) a more complex overall dynamic is observed (see Figure 10). Within 3470 cm^{-1}-3630 cm^{-1} the time at which the maximum band intensity is reached decreases from about 107 s to 95 s, i.e., bridged hydroxyl species (at < 3600 cm^{-1}) show their maximum intensity considerably later than terminal hydroxyl groups (at > 3600 cm^{-1}). By using a sine function for the PSD (see equation 2), the time values of the minima of the bands always occur shifted by half a period relative to the time values of the maxima. Since the maxima of the bridged hydroxyl groups show their maximum at larger time values, this indicates that during the surface reaction, terminal hydroxyl groups are consumed, before bridged hydroxyl groups.

Terminal hydroxyl bands located at higher wavenumbers, i.e., within 3650-3700 cm^{-1}, also show dynamics to some extent. In contrast to the hydroxyl bands considered above, these bands did not show their maximum intensity during the second, but already during the first half-period after about 19.3±2.7 s. Thus, the corresponding hydroxyl species are not consumed but formed on the timescale of the formation of C–H adsorbates or slightly before. The hydroxyl band at 3657 cm^{-1} exhibits its maximum after 19.0±2.0 s, the band at 3677 cm^{-1} after 21.6±2.9 s and the band at 3690 cm^{-1} after 17.3±3.1 s. In contrast to the C–H vibrations bands, these features show overlapping error bars and therefore cannot be conclusively assigned to hydroxyl species formed at different times, as the standard deviation in the time values of these bands is too high compared to the time between two DRIFT spectra.

For the δ(Sn-OH) band at 934 cm^{-1}, the low band intensity and/or signal-to-noise ratio in the PSD spectra results in a large error in the time value, preventing an assignment to a specific hydroxyl species (see Figure S3). However, a comparison with the bands at 979 cm^{-1} and 1247 cm^{-1}, which can also be assigned to δ(Sn-OH)-vibration bands of terminal hydroxyl-groups, is feasible.[3,4,56,57] These two bands have time values Δt of 23.3±5.0 s and 15.4±3.8 s, respectively, thus showing their maximum intensity in the first half-period. The occurrence of hydroxyl bands with maxima in the first half-period indicates, that hydroxyl groups not only participate in the reaction with ethanol, resulting in the formation of ethoxy-species and consumption of hydroxy species, but may also be involved in other reaction steps, leading to the formation of hydroxyl-groups, e.g., the formation of acetaldehyde by dehydration or oxidative dehydration, where hydrogen atoms could be accepted by oxygen and hydroxyl species. Alternatively, during adsorption of ethanol hydrogen

atoms may be transferred to a hydroxyl- or oxygen species next to the ethanol adsorption site, leading to the formation of ethoxy species and new hydroxyl species. The latter scenario could especially be true for the hydroxyl species, characterized by the bands at 979 cm^{-1} and 3677 cm^{-1}, which has its maxima at similar time values as the ethanol and ethoxy-related C-H species.

4. Influence of Gold-Loading and Proposed Mechanism

For the measurements of the resistance as a function of oxygen partial pressure, a decrease in the exponent *n* was observed with increasing gold loading. It was also found that the resistance of the sensors steadily increased with the gold loading, especially at low volume fractions of oxygen. These observations lead to the following important findings: The resistance of the sensor is dependent on the oxygen partial pressure, as correctly predicted by equations 5 and 6, both for unloaded and gold-loaded samples. This dependence is considerably affected by the gold loading, even at very low loadings, such as 0.1 wt% Au. Such a behavior was also observed previously for tin oxide used as a gas sensor material for CO detection.[6] Loading SnO_2 with gold further leads to a large increase in the absolute resistance value, which is also observed in synthetic air without the presence of ethanol. Thus, an exclusive spillover of the analyte to explain the increase in sensor response can be excluded, since changes in the sensor properties are detected even in the absence of ethanol. A clear influence of the gold loading on the sensor response is apparent in the temperature-dependent measurements using synthetic air as the carrier gas (see Figure 3a). While bare SnO_2 showed a steady decrease in sensor response with increasing temperature, the sensor response passed through a maximum in the case of the gold-loaded samples. Since the resistances during ethanol exposure were higher than that of bare tin oxide at all temperatures studied (see Figure 3b), the increase in sensor response is attributed to the interaction of gold with oxygen rather than ethanol. Besides, with increasing volume fraction of oxygen, the resistances of the gold-loaded samples were observed to be higher than those of bare tin oxide (see Figure 4), indicating that the activity of the sensor surface is influenced by gold even before the actual sensor reaction. This behavior may be caused either by an electronic effect or by the interaction of gold with the gas environment, i.e., oxygen. The interaction with nitrogen should be negligible because it is chemically inert.

The XPS and UV-Vis results in Figure 2 contradict an electronic effect as gold is present in metallic form. No significant change was observed when comparing the X-ray powder diffractograms of bare and gold-loaded tin oxide (see Figure S1). The conclusion regarding the presence of metallic gold particles on the surface is also supported by literature results obtained by high energy resolution fluorescence-detected XANES (HERFD-XANES) for gold-loaded tin oxide,[13] especially in comparison with platinum- and palladium-loaded tin oxide.[16,58] Simultaneous DC resistance and work function change measurements by HÜBNER *et al.* further support the exclusion of an

electronic effect of gold based on Fermi-level control of the sensor resistance, because bare and gold-loaded tin oxide show the same dependence of the DC resistance and the work function change for oxidizing and reducing gases.[13]

In the case of oxygen spillover from gold to the surface of tin oxide, an increase in resistance could occur without any change in the properties of gold. In fact, oxygen spillover would be accompanied by an increased concentration of oxygen species on the surface, which in turn would affect the electron density in the conduction band. As a result, we would expect an increase in the resistance of the gold-loaded samples with gold loading, which is fully consistent with the observed behavior.

Further evidence for an increased oxygen concentration was also provided by the lower intensity of C–H-containing adsorbates for gold-loaded tin oxide compared to bare tin oxide during ethanol exposure (see Figure 6a), which can be attributed to the enhanced oxidation to acetaldehyde and CO_2 in the presence of gold. Furthermore, the integrated intensity of the sum of OH bands showed a smaller change for the gold-loaded samples than for the unloaded samples because oxygen and hydroxyl species provided and formed by oxygen spillover are preferentially consumed (see Figures 5a and 7a). These effects of the gold loading on the band intensity of surface species involved in the sensor mechanism are mainly observed when oxygen is present in the gas phase, further highlighting the importance of the interaction of oxygen with metallic gold.

Finally, based on the findings of this study as well as previous results by ELGER AND HESS,[5,18] we propose a mechanism for ethanol gas sensing over gold-loaded tin oxide. The mechanism is dominated by the consumption of hydroxyl groups, as well as the formation of surface adsorbates such as ethoxy, acetate, and formate. Acetaldehyde, water, and CO_2 were observed as gas-phase products of the oxidation of ethanol. In contrast to the mechanism postulated by ELGER AND HESS,[5,18] which is mainly based on *operando* Raman and UV-Vis spectra, in this work carboxylates and carbonates were observed as additional surface species by using DRIFTS. The concentration of carboxylates and carbonates decreased during ethanol exposure but increased during the regeneration phase as revealed by the MES measurements, strongly suggesting that carboxylates and carbonates are formed by the decomposition of adsorbates or re-adsorption of CO_2 from the gas phase.
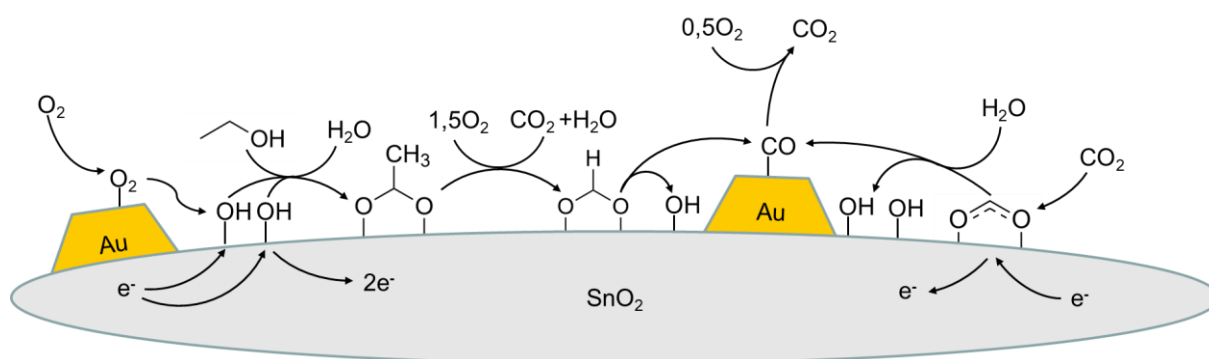
Figure 11. Proposed mechanism of ethanol gas sensing over gold-loaded tin oxide considering the surface species observed by transient IR spectroscopy. For clarity, the formation and reoxidation of oxygen vacancies is not included in the Figure, but is not excluded to take place. For details see text.

Figure 11 illustrates the most important steps of the postulated mechanism of ethanol gas sensing over gold-loaded tin oxide, supported by the results obtained in this study. As mentioned previously, molecular oxygen is first adsorbed on the surface of the gold particles and then spilled over onto the tin oxide surface. The resulting adsorbed oxygen has previously been proposed to be present as molecular or atomic surface adsorbates[59,60], but such isolated, charged adsorbed oxygen species (e.g. O_2^{2-}, O_2^-), have not been detected for tin oxide by spectroscopic methods under *operando* conditions yet[5,42,59]. Hydroxyl species, on the other hand, have been observed under *operando* conditions in several studies,[4,5,35] and were also observed in this work (see Table S3). In fact, hydroxyl species show a pronounced temporal development in band intensity when ethanol is added, as well as when the addition of ethanol is stopped and the sensor material is regenerated in the presence of oxygen. Therefore, in Figure 11 the adsorbed oxygen from spillover is proposed to transform into hydroxyl-type species as reactive surface species on the sensor material tin oxide. These newly-formed hydroxyl-type species can accept electrons from the conduction band of the tin oxide, leading to an increase in the resistance of the tin oxide. Hydrogen necessary for the formation of these hydroxyl-type species could be provide by reaction with water pre-adsorbed on the surface or transport and donation of hydrogen by hydroxyl-species on the surface. It should be kept in mind, that the conversion of ethanol also provides hydrogen for subsequent modulation periods. Hydroxyl species in proximity to the gold particles could form hydroxyl-type species with spilled oxygen, in which several oxygen atoms share a hydrogen atom in a hydrogen bond-like situation to stabilize otherwise ionic states by forming polar bonds of covalent nature.

Alternatively to these proposed hydroxyl-type species, oxygen surface lattice sites could be formed by reoxidation of oxygen vacancies, consuming oxygen provided by oxygen spillover.[11,42] Such newly formed oxygen lattice sites could alternatively act as reaction sites for ethanol gas conversion during gas sensing., as shown by DEGLER *et al*. for CO gas sensing on SnO_2[4,42] and

Au/SnO$_2$[6]. However, intensity changes of bands related to this surface lattice oxygen species were not observed during our ME measurements. This could be attributed to the poor signal-to-noise ratio in the range below 1200 cm^{-1}, masking the corresponding bands. Besides, the corresponding vibrational bands may overlap to some degree with the deformation modes of the hydroxyl-type species, as well as the features of carbonate and carboxylate species. On the other hand, it cannot be excluded that after an initial reduction of the material due to the consumption of oxygen surface lattice sites, they are no longer actively involved in the mechanism of ethanol gas sensing within the modulation of the ethanol concentration, and thus do not show any intensity changes in the PSD spectra. Nevertheless, as also suggested by DEGLER *et al.*[4,61] and other researchers[25,39], surface oxygen lattice sites and different types of hydroxyl-groups are connected by several equilibrium reactions. Hence, a decrease in hydroxyl-type species could also be connected to a decrease in surface oxygen lattice sites and vice versa. Because of this, our results do not contradict the formation and consumption of surface oxygen lattice sites, under the assumption, that both gas sensing mechanisms (ethanol, CO) involve the same reactive surface sites in their respective mechanism, despite their clear difference in molecular structure and chemical behavior. In any case, our ME-DRIFTS results do not provide any evidence for the contribution of such species.

Upon exposure to the analyte, the hydroxyl-type species are consumed by reaction with ethanol, releasing electrons back into the conduction band, as shown by the time-resolved DRIFTS measurements in Figures 5 and 7, as well as the MES measurements in Figure 10. Detailed analysis of the time values Δt reveals (see Figure 10) that hydroxyl groups can also act as hydrogen acceptors during the formation of ethoxy species or acetaldehyde, followed by their desorption as water or transport between different surface sites. Adsorbed ethanol is then further oxidized to ethoxy and acetate, or, by further oxidation, to formate. The formation of these oxidized surface adsorbates could be identified by their time values Δt (24.2±0.9 s), which deviated from the time values Δt of adsorbed ethanol (21.8±0.5 s). Formate, carbonate and carboxylates can possibly dissociate near gold particles, forming CO and new hydroxyl groups. CO adsorbed on negatively charged gold particles was accessible by transient spectroscopy, showing its maximum at a time value Δt in the second half-period (~100 s), which is significantly later than the maxima of ethanol and other C–H-containing groups. Coupled to the formation of CO, new hydroxyl groups are formed, supporting the regeneration of the tin oxide surface in the second half-period. CO adsorbed on gold particles reacts with oxygen from the gas phase to form CO$_2$. Part of the CO$_2$ resulting from the oxidation of ethoxy, formate or acetate species can re-adsorb on the surface of tin oxide, forming carboxylates (see Figure 11) or carbonates (not shown here) by accepting electrons from the conduction band. These species also show their maximum in the second half-period ($\Delta t \simeq 92$ s), before the maximum of CO on gold particles, leading to the conclusion that they are also involved in the formation of CO and are formed by CO$_2$.

5. Conclusions

The combination of resistance measurements and DRIFTS, in particular by using the modulation excitation (ME) method, provides new insight into the mechanism of ethanol gas sensing over tin oxide-based sensors and the role of gold. It is demonstrated that the IR spectroscopic methods used provide complementary information on surface processes of tin oxide gas sensors. Based on the results of the IR spectroscopic measurements, a mechanism for ethanol gas sensing over gold-loaded tin oxide was postulated, which involves an oxygen spillover to activate the tin oxide surface by formation of adsorbed oxygen, followed by the reaction to acetate and formate, and its decomposition, leading to CO adsorption on gold. The use of ME-DRIFTS, which detects species actively participating in the reaction processes, enabled the detection of this CO species for the first time, besides the discrimination of other adsorbates from a broad C–H-related band based on their different temporal behavior.

For a more detailed mechanistic picture, the resistance and IR measurements were complemented by XPS and UV-Vis spectroscopy, providing information on the electronic properties of gold supported on tin oxide. Gold was found to be present exclusively in its metallic state, not affecting the electronic properties of tin oxide through electronic coupling or formation of gold oxides. These findings underline the proposed mechanism of oxygen spillover in the presence of gold when oxygen from the gas phase is available. The resulting increase in the concentration of oxygen on the sensor surface then results in an increase in the sensor resistance in the absence of ethanol and an increase in the sensor response S in the presence of ethanol. Thus, based on the resistance and spectroscopic measurements, we developed a fully consistent picture of the role of gold for ethanol gas sensing.

By using ME-DRIFTS in combination with the novel analysis approach outlined in this study, also other oxide-based gas-sensing materials should be readily accessible to transient spectroscopic studies. We expect that the application of ME-DRIFTS together with PSD will open exciting possibilities for studying the mechanistic details of metal oxide gas sensors in the future, including the detection of new intermediates and the elucidation of their dynamical behavior.

Supporting Information

Results of sample characterization (XRD, XPS, ICP-OES) and further analyses; additional DRIFT and PSD spectra; summary of vibrational band assignments.

Conflicts of interest: The authors declare no conflict of interest.

References

(1) Bonne, U. Gas Sensors. In *Comprehensive microsystems*; Gianchandani, Y. B., Ed.; Elsevier: Amsterdam, 2008; pp 375–432.

(2) Tiemann, M. Porous metal oxides as gas sensors. *Chem. Eur. J.* **2007**, *13*, 8376–8388.

(3) Koziej, D.; Thomas, K.; Barsan, N.; Thibault-Starzyk, F.; Weimar, U. Influence of annealing temperature on the CO sensing mechanism for tin dioxide based sensors–Operando studies. *Catal. Today* **2007**, *126*, 211–218.

(4) Degler, D.; Junker, B.; Allmendinger, F.; Weimar, U.; Barsan, N. Investigations on the Temperature-Dependent Interaction of Water Vapor with Tin Dioxide and Its Implications on Gas Sensing. *ACS Sens.* **2020**, *5*, 3207–3216.

(5) Elger, A.-K.; Hess, C. Elucidating the Mechanism of Working SnO_2 Gas Sensors Using Combined Operando UV/Vis, Raman, and IR Spectroscopy. *Angew. Chem. Int. Ed.* **2019**, *58*, 15057–15061.

(6) Degler, D.; Rank, S.; Müller, S.; Pereira de Carvalho, H. W.; Grunwaldt, J.-D.; Weimar, U.; Barsan, N. Gold-Loaded Tin Dioxide Gas Sensing Materials: Mechanistic Insights and the Role of Gold Dispersion. *ACS Sens.* **2016**, *1*, 1322–1329.

(7) Itoh, T.; Nakashima, T.; Akamatsu, T.; Izu, N.; Shin, W. Nonanal gas sensing properties of platinum, palladium, and gold-loaded tin oxide VOCs sensors. *Sens. Actuators B* **2013**, *187*, 135–141.

(8) Yamazoe, N.; Kurokawa, Y.; Seiyama, T. Effects of additives on semiconductor gas sensors. *Sens. Actuators B* **1983**, *4*, 283–289.

(9) Matsushima, S.; Teraoka, Y.; Miura, N.; Yamazoe, N. Electronic Interaction between Metal Additives and Tin Dioxide in Tin Dioxide-Based Gas Sensors. *Jpn. J. Appl. Phys.* **1988**, *27*, 1798–1802.

(10) Yamazoe, N. New approaches for improving semiconductor gas sensors. *Sens. Actuators B* **1991**, *5*, 7–19.

(11) Degler, D.; Weimar, U.; Barsan, N. Current Understanding of the Fundamental Mechanisms of Doped and Loaded Semiconducting Metal-Oxide-Based Gas Sensing Materials. *ACS Sens.* **2019**, *4*, 2228–2249.

(12) McAleer, J. F.; Moseley, P. T.; Norris, J. O. W.; Williams, D. E.; Tofield, B. C. Tin dioxide gas sensors. Part 2.—The role of surface additives. *J. Chem. Soc., Faraday Trans. 1* **1988**, *84*, 441.

(13) Hübner, M.; Koziej, D.; Grunwaldt, J.-D.; Weimar, U.; Barsan, N. An Au clusters related spill-over sensitization mechanism in SnO_2-based gas sensors identified by operando HERFD-XAS, work function changes, DC resistance and catalytic conversion studies. *Phys. Chem. Chem. Phys.* **2012**, *14*, 13249–13254.

(14) Staerz, A.; Boehme, I.; Degler, D.; Bahri, M.; Doronkin, D. E.; Zimina, A.; Brinkmann, H.; Herrmann, S.; Junker, B.; Ersen, O.*; et al.* Rhodium Oxide Surface-Loaded Gas Sensors. *Nanomaterials* **2018**, *8*.

(15) Staerz, A.; Kim, T.-H.; Lee, J.-H.; Weimar, U.; Barsan, N. Nanolevel Control of Gas Sensing Characteristics via p–n Heterojunction between Rh_2O_3 Clusters and WO_3 Crystallites. *J. Phys. Chem. C* **2017**, *121*, 24701–24706.

(16) Hübner, M.; Koziej, D.; Bauer, M.; Barsan, N.; Kvashnina, K.; Rossell, M. D.; Weimar, U.; Grunwaldt, J.-D. The Structure and Behavior of Platinum in SnO_2 -Based Sensors under Working Conditions. *Angew. Chem. Int. Ed.* **2011**, *50*, 2841–2844.

(17) Morrison, S. Selectivity in semiconductor gas sensors. *Sens. Actuators B* **1987**, *12*, 425–440.

(18) Elger, A.-K.; Hess, C. Application of Raman Spectroscopy to Working Gas Sensors: From in situ to operando Studies. *Sensors* **2019**, *19*, 5075–5091.

(19) Sänze, S.; Hess, C. Ethanol Gas Sensing by Indium Oxide: An Operando Spectroscopic Raman-FTIR Study. *J. Phys. Chem. C* **2014**, *118*, 25603–25613.

(20) Liu, C.; Kuang, Q.; Xie, Z.; Zheng, L. The effect of noble metal (Au, Pd and Pt) nanoparticles on the gas sensing performance of SnO_2 -based sensors: a case study on the {221} high-index faceted SnO_2 octahedra. *CrystEngComm* **2015**, *17*, 6308–6313.

(21) van Bokhoven, J. A.; Miller, J. T. d Electron Density and Reactivity of the d Band as a Function of Particle Size in Supported Gold Catalysts. *J. Phys. Chem. C* **2007**, *111*, 9245–9249.

(22) Baurecht, D.; Fringeli, U. P. Quantitative modulated excitation Fourier transform infrared spectroscopy. *Rev. Sci. Instrum.* **2001**, *72*, 3782–3792.

(23) Urakawa, A.; Bürgi, T.; Baiker, A. Sensitivity enhancement and dynamic behavior analysis by modulation excitation spectroscopy: Principle and application in heterogeneous catalysis. *Chem. Eng. Sci.* **2008**, *63*, 4902–4909.

(24) Srinivasan, P. D.; Patil, B. S.; Zhu, H.; Bravo-Suárez, J. J. Application of modulation excitation-phase sensitive detection-DRIFTS for in situ/ operando characterization of heterogeneous catalysts. *React. Chem. Eng.* **2019**, *4*, 862–883.

(25) Pavelko, R. G.; Choi, J.-K.; Urakawa, A.; Yuasa, M.; Kida, T.; Shimanoe, K. H_2O/D_2O Exchange on SnO_2 Materials in the Presence of CO: Operando Spectroscopic and Electric Resistance Measurements. *J. Phys. Chem. C* **2014**, *118*, 2554–2563.

(26) Müller, P.; Hermans, I. Applications of Modulation Excitation Spectroscopy in Heterogeneous Catalysis. *Ind. Eng. Chem. Res.* **2017**, *56*, 1123–1136.

(27) Aguirre, A.; Collins, S. E. Selective detection of reaction intermediates using concentration-modulation excitation DRIFT spectroscopy. *Catal. Today* **2013**, *205*, 34–40.

(28) Bürgi, T.; Baiker, A. In Situ Infrared Spectroscopy of Catalytic Solid–Liquid Interfaces Using Phase-Sensitive Detection: Enantioselective Hydrogenation of a Pyrone over Pd/TiO_2. *J. Phys. Chem. B* **2002**, *106*, 10649–10658.

(29) Patterson, A. L. The Scherrer Formula for X-Ray Particle Size Determination. *Phys. Rev.* **1939**, *56*, 978–982.

(30) Moulder, J. F.; Chastain, J., Eds. *Handbook of X-ray photoelectron spectroscopy: A reference book of standard spectra for identification and interpretation of XPS data*; Perkin-Elmer Corporation: Eden Prairie, Minn., 1992.

(31) Manjula, P.; Arunkumar, S.; Manorama, S. V. Au/SnO_2 an excellent material for room temperature carbon monoxide sensing. *Sens. Actuators B* **2011**, *152*, 168–175.

(32) Kreibig, U.; Genzel, L. Optical absorption of small metallic particles. *Surf. Sci.* **1985**, *156*, 678–700.

(33) Maier, J. *Physical chemistry of ionic materials: Ions and electrons in solids*; Wiley: Chichester, Hoboken, NJ, 2004.

(34) Barsan, N.; Weimar, U. Conduction Model of Metal Oxide Gas Sensors. *J. Electroceram.* **2001**, *7*, 143–167.

(35) Amalric-Popescu, D.; Bozon-Verduraz, F. Infrared studies on SnO_2 and Pd/SnO_2. *Catal. Today* **2001**, *70*, 139–154.

(36) Harbeck, S.; Szatvanyi, A.; Barsan, N.; Weimar, U.; Hoffmann, V. DRIFT studies of thick film un-doped and Pd-doped SnO_2 sensors: temperature changes effect and CO detection mechanism in the presence of water vapour. *Thin Solid Films* **2003**, *436*, 76–83.

(37) Raskó, J.; Hancz, A.; Erdőhelyi, A. Surface species and gas phase products in steam reforming of ethanol on TiO_2 and Rh/TiO_2. *Appl. Catal. A-Gen* **2004**, *269*, 13–25.

(38) Harrison, P. G.; Guest, A. Tin oxide surfaces. Part 18.—Infrared study of the adsorption of very low levels (20–50 ppm) of carbon monoxide in air on to tin (IV) oxide gel. *J. Chem. Soc., Faraday Trans. 1* **1989**, *85*, 1897.

(39) Wicker, S.; Guiltat, M.; Weimar, U.; Hémeryck, A.; Barsan, N. Ambient Humidity Influence on CO Detection with SnO_2 Gas Sensing Materials. A Combined DRIFTS/DFT Investigation. *J. Phys. Chem. C* **2017**, *121*, 25064–25073.

(40) Thornton, E. W.; Harrison, P. G. Tin oxide surfaces. Part 3.—Infrared study of the adsorption of some small organic molecules on tin(IV) oxide. *J. Chem. Soc., Faraday Trans. 1* **1975**, *71*, 2468.

(41) Pei, Z.-F.; Ponec, V. On the intermediates of the acetic acid reactions on oxides: an IR study. *Appl. Surf. Sci.* **1996**, *103*, 171–182.

(42) Degler, D.; Wicker, S.; Weimar, U.; Barsan, N. Identifying the Active Oxygen Species in SnO_2 Based Gas Sensing Materials: An Operando IR Spectroscopy Study. *J. Phys. Chem. C* **2015**, *119*, 11792–11799.

(43) Tan, T. H.; Scott, J.; Ng, Y. H.; Taylor, R. A.; Aguey-Zinsou, K.-F.; Amal, R. C–C Cleavage by Au/TiO_2 during Ethanol Oxidation: Understanding Bandgap Photoexcitation and Plasmonically Mediated Charge Transfer via Quantitative in Situ DRIFTS. *ACS Catal.* **2016**, *6*, 8021–8029.

(44) Wang, J.; Kispersky, V. F.; Nicholas Delgass, W.; Ribeiro, F. H. Determination of the Au active site and surface active species via operando transmission FTIR and isotopic transient experiments on 2.3wt.% Au/TiO_2 for the WGS reaction. *J. Catal.* **2012**, *289*, 171–178.

(45) Boccuzzi, F.; Chiorino, A.; Manzoli, M.; Andreeva, D.; Tabakova, T. FTIR Study of the Low-Temperature Water–Gas Shift Reaction on Au/Fe_2O_3 and Au/TiO_2 Catalysts. *J. Catal.* **1999**, *188*, 176–185.

(46) Boronat, M.; Corma, A. Oxygen activation on gold nanoparticles: separating the influence of particle size, particle shape and support interaction. *Dalton Trans.* **2010**, *39*, 8538–8546.

(47) Carabineiro, S. A. C.; Nieuwenhuys, B. E. Adsorption of small molecules on gold single crystal surfaces. *Gold Bull.* **2009**, *42*, 288–301.

(48) Raskó, J.; Kecskés, T.; Kiss, J. FT-IR and mass spectrometric studies on the interaction of acetaldehyde with TiO_2-supported noble metal catalysts. *Appl. Catal. A-Gen* **2005**, *287*, 244–251.

(49) Lyalin, A.; Taketsugu, T. Adsorption of Ethylene on Neutral, Anionic, and Cationic Gold Clusters. *J. Phys. Chem. C* **2010**, *114*, 2484–2493.

(50) Futamata, M.; Diesing, D. Adsorbed state of pyridine, uracil and water on gold electrode surfaces. *Vib. Spectrosc.* **1999**, *19*, 187–192.

(51) Manzoli, M.; Chiorino, A.; Vindigni, F.; Boccuzzi, F. Hydrogen interaction with gold nanoparticles and clusters supported on different oxides: A FTIR study. *Catal. Today* **2012**, *181*, 62–67.

(52) Boccuzzi, F.; Chiorino, A.; Manzoli, M. FTIR study of the electronic effects of CO adsorbed on gold nanoparticles supported on titania. *Surf. Sci.* **2000**, *454-456*, 942–946.

(53) Song, H.; Bao, X.; Hadad, C. M.; Ozkan, U. S. Adsorption/Desorption Behavior of Ethanol Steam Reforming Reactants and Intermediates over Supported Cobalt Catalysts. *Catal. Lett.* **2011**, *141*, 43–54.

(54) Chieregato, A.; Velasquez Ochoa, J.; Bandinelli, C.; Fornasari, G.; Cavani, F.; Mella, M. On the chemistry of ethanol on basic oxides: revising mechanisms and intermediates in the Lebedev and Guerbet reactions. *ChemSusChem* **2015**, *8*, 377–388.

(55) Sänze, S.; Gurlo, A.; Hess, C. Monitoring Gas Sensors at Work: Operando Raman-FTIR Study of Ethanol Detection by Indium Oxide. *Angew. Chem. Int. Ed.* **2013**, *52*, 3607–3610.

(56) Orel, B.; Lavrenčič-Štankgar, U.; Crnjak-Orel, Z.; Bukovec, P.; Kosec, M. Structural and FTIR spectroscopic studies of gel-xerogel-oxide transitions of SnO_2 and SnO_2:Sb powders and dip-coated films prepared via inorganic sol-gel route. *J. Non-Cryst. Solids* **1994**, *167*, 272–288.

(57) Thornton, E. W.; Harrison, P. G. Tin oxide surfaces. Part 1.—Surface hydroxyl groups and the chemisorption of carbon dioxide and carbon monoxide on tin(IV) oxide. *J. Chem. Soc., Faraday Trans. 1* **1975**, *71*, 461.

(58) Koziej, D.; Hübner, M.; Barsan, N.; Weimar, U.; Sikora, M.; Grunwaldt, J.-D. Operando X-ray absorption spectroscopy studies on Pd-SnO_2 based sensors. *Phys. Chem. Chem. Phys.* **2009**, *11*, 8620.

(59) Gurlo, A. Interplay between O_2 and SnO_2: oxygen ionosorption and spectroscopic evidence for adsorbed oxygen. *ChemPhysChem* **2006**, *7*, 2041–2052.

(60) Sun, Y.-F.; Liu, S.-B.; Meng, F.-L.; Liu, J.-Y.; Jin, Z.; Kong, L.-T.; Liu, J.-H. Metal oxide nanostructures and their gas sensing properties: a review. *Sensors* **2012**, *12*, 2610–2631.

(61) Tofighi, G.; Degler, D.; Junker, B.; Müller, S.; Lichtenberg, H.; Wang, W.; Weimar, U.; Barsan, N.; Grunwaldt, J.-D. Microfluidically synthesized Au, Pd and AuPd nanoparticles supported on SnO_2 for gas sensing applications. *Sens. Actuators B* **2019**, *292*, 48–56.